Carbon 178 (2021) 803–809

Contents lists available at ScienceDirect

Carbon

journal homepage: www.elsevier.com/locate/carbon

Passive UHF RFID tags made with graphene assembly film-based antennas

Bohan Zhang [a, b], Zhe Wang [a], Rongguo Song [a, b], Huaqiang Fu [c], Xin Zhao [a], Cheng Zhang [a], Daping He [a, c, *], Zhi P. Wu [a, b, **]

[a] Hubei Engineering Research Center of RF-Microwave Technology and Application, Wuhan University of Technology, Wuhan, 430070, PR China
[b] School of Information Engineering, Wuhan University of Technology, Wuhan, 430070, PR China
[c] State Key Laboratory of Silicate Materials for Architectures, Wuhan University of Technology, Wuhan, 430070, PR China

ARTICLE INFO

Article history:
Received 4 October 2020
Received in revised form
22 February 2021
Accepted 26 February 2021
Available online 19 March 2021

Keywords:
UHF RFID
Graphene film
High conductivity
Mechanical stability

ABSTRACT

Ultra-high frequency (UHF) radio frequency identification (RFID) tags with an antenna made of a highly flexible graphene assembly film (GAF) is presented. The superb electrical conductivity (~1.6×10^6 S m^{-1}) of the GAF results in the tag to reach reading range of ~12 m, which is comparable to that of the commercially available metallic counterparts. The performance of the GAF-based RFID tags under mechanical bending and stretching is experimentally evaluated, which demonstrates excellent mechanical stability of the GAF tag than that of metallic tags. Additionally, substrate stability tests are also conducted. The GAF-based UHF RFID tags can thus lead to numerous applications in information exchange, tracking and tracing as well as the Internet of Things (IoT).

1. Introduction

Ultra-high frequency (UHF) radio frequency identification (RFID) technology is the perceptual layer in information collection in Internet of Things (IoT) applications. Due to its fascinating properties of passive, low cost, long read range and unique identification, RFID technology has been implemented for various applications, including but not limited to healthcare, logistics, smart shopping and public safety [1–4]. With respect to an RFID system, the antenna is a key component, therefore, tremendous work related to the design and optimization of the antenna for achieving remote tracking and intelligent monitoring under various conditions [5–7], has been motivated. Generally metallic materials such as copper and aluminum are adopted for building the RFID antennas, in which the fabrication process including chemical etching and printed circuit board is cumbersome and not environmental-friendly. Moreover, metallic tags show poor mechanical, chemical and thermal stability, resulting in the destruction of massive tags and the generation of electronic waste in IoT applications [8,9]. Hence, the replacement of metals by environmentally friendly and robust materials with high conductivity is extremely urgent and appealing to industries.

Carbon-based materials including carbon nanotubes, carbon fibers and graphite films are of increasing attention in the manufacture of antennas owing to their superb flexibility and lightweight compared to traditional metals [10–14]. These materials, however, have rarely been used in antennas of UHF RFID tags mainly due to their unsatisfactory electrical conductivity. Graphene, as the thinnest two-dimensional (2D) atomic crystal composed of pure carbon atoms arranged in hexagonal honeycomb lattice [15–18], could ideally exhibit a superb conductivity of ~10^8 S m^{-1} and has been demonstrated to be applicable in terahertz (THz) range [19,20]. Due to the high sheet resistance (~30 Ω) and the ohmic losses caused by the extremely thin 2D atomic structure, its applications in the microwave region have been limited [21,22]. In contrast to single layer graphene, graphene-based films [23–25] are made of graphene-related materials such as graphene nanoplatelets (GNP), graphene oxide (GO) and reduced graphene oxide (rGO), have been adopted as alternative conductive materials

* Corresponding author. Hubei Engineering Research Center of RF-Microwave Technology and Application, School of Science, Wuhan University of Technology, Wuhan, 430070, PR China.
** Corresponding author. Hubei Engineering Research Center of RF-Microwave Technology and Application, Wuhan University of Technology, Wuhan, 430070, PR China.
E-mail addresses: hedaping@whut.edu.cn (D. He), z.p.wu@whut.edu.cn (Z.P. Wu).

https://doi.org/10.1016/j.carbon.2021.02.096
0008-6223/

[26–36]. Most recently, graphene inks have been produced with the conductivity of 3.7 × 10^4 S m^{-1} for printable IoT antenna applications [32]. However, some certain additives including solvent, binder and dispersant are required to form a continuous film which limit the conductivity of the graphene inks. A graphene paper with conductivity up to 4.2 × 10^5 S m^{-1} has been reported for short range [36], near field communication (NFC) applications at high frequency, while the successful application of graphene paper in UHF RFID is still hard to accomplish due to the un-matching conductivity compared to traditional metals. We have reported the successful synthesis of a multi-layered graphene film with conductivity up to 10^6 S/m in the applications of filter and sensor [37,38].

Here, we report a UHF RFID tag with an antenna based on high conductivity graphene assembly film (GAF), which can achieve a comparable read range of the commercially available metallic antennas. The GAF endowed with superb flexibility, lightweight and outstanding mechanical stability plus durability gives the GAF-based RFID tag with numerous desirable features that cannot be accomplished by the traditional types. Bending and stretching tests are performed demonstrating excellent mechanical stability of the fabricated GAF tags. Application scenarios including five substrates are also tested which shows promising results.

2. Experimental

2.1. GAF preparation and characteristics measurement

The GO suspension was diluted with ultrapure water to a concentration of 15 mg mL^{-1} in a square vessel. After mechanical stirring at room temperature, the diluted GO suspension was evaporated to obtain the GO film. The GO film was annealed in Ar gas flows furnace at a high temperature of 1300 °C and 3000 °C for 2 h and 1 h, respectively, achieving the reduction and graphitization of the GAF. Then the GAF was attached to the PET substrate by static calendaring with the pressure of 100 MPa for 0.5 h at room temperature. Raman spectroscopy was performed using a Renishaw Raman Spectrometer. SEM and TEM were acquired with a JSM-7100F and JEM-2100F, respectively. XRD patterns were collected using X-ray D/MAX-RB instruments by Cu Ka radiation. Conductivity and sheet resistance were measured via a Four-Point Probes Resistivity Measurement System (RTS-9).

2.2. GAF antennas fabrication and measurement

The GAF antennas were modeled and optimized using the CST full wave simulation software. In the simulation, the conductivity and thickness of the GAF were assumed to be constant. The GAF antenna was affixed to the PET substrate, the substrate thickness is 0.05 mm, the dielectric constant is 3.9, and the tangential loss is 0.003. The PET substrate has flexibility, high temperature resistance and chemical stability, which can support and protect the antenna. The optimized design was selected based on the simulated results of complex impedance, realized gain, radiation efficiency and radiation pattern. The GAF was patterned accurately using the LPKF laser machine with the programed path. After the redundant GAF was peeled off, GAF antennas were formed. In the two-port complex impedance measurement of the antennas [39], the test fixture consisted of two semi-rigid coaxial cables. On one end of the test fixture, the outer conductors were soldered together and the inner conductors were connected to the antenna using conductive epoxy (Circuit works CW2400). On the other end, the test fixture was connected to the vector network analyzer (VNA, Agilent E5072A) using two Sub-Miniature version A (SMA) connectors and the two cables. After two ports extension, the antenna measured complex impedance Z_a is given by:

$$Z_a = \frac{2Z_0(1 - S_{11}S_{22} + S_{12}S_{21} - S_{12} - S_{21})}{(1 - S_{11})(1 - S_{22}) - S_{21}S_{12}} \quad (1)$$

where $Z_0 = 50\ \Omega$. S_{11}, S_{12}, S_{21} and S_{22} are four measured S parameters of two ports, represented in the plural. The realized gain and radiation efficiency measurements were performed using the VNA, Diamond Engineering Antenna Measurement Studio and rotary table in the anechoic chamber.

2.3. GAF tag fabrication and read range measurement

The GAF antennas could be transferred onto various flexible substrates, such as PET, polyimide (PI), polyvinyl chloride (PVC), coated paper and so on. The chips of Impinj Monza R6 series were connected to the GAF antennas with anisotropic conductive heat-curing adhesive Delo AC265. The adhesive dispending and flip chips bonding were performed by a semi-automatic packaging machine. After being laminated with the various face stocks printed with exclusive information, the GAF tag fabrication was completed. Tag read range measurement was performed using Voyantic Tagformance Pro RFID Measurement System in anechoic chamber. The default value of *EIRP* was 3.28 W in China and Europe, for countries that allow 4.00 W *EIRP*, the measurement result needs to be increased by 11%. The reader has a linear polarization patch antenna, the transmit power range of reader was 0 dB m to 27 dB m, and the receiver had a sensitivity of −75 dB m. The forward loss denoted with L_{fwd} includes free space and cable loss. L_{fwd} was measured during calibration to eliminate the effect of cable loss. The measured threshold power is represented by P_{th}. The transmit power was increased in 0.1 dB m steps until the test tag was activated, at which point the transmit power value was P_{th}. Then, a valid response was received from tag to an inquiry command for the Electronic Product Code (EPC) Type 1 Gen 2 protocol. The frequency was swept from 800 MHz to 1000 MHz in a step of 1 MHz. The tag read range R_t is defined as the maximum distance that the tag can be read forward in the free space [40], which can be calculated according to the Friss formula:

$$R_t = \frac{\lambda}{4\pi}\sqrt{\frac{P_r G_r G_t}{P_t}} = \frac{\lambda}{4\pi}\sqrt{\frac{EIRP \cdot G_t \cdot \tau}{P_c}} = \frac{\lambda}{4\pi}\sqrt{\frac{EIRP}{P_{th} L_{fwd}}} \quad (2)$$

where λ is the wavelength at the operating frequency in the free space. P_r, G_r, P_t, and G_t are the radiated power and realized gain of reader and tag, respectively. *EIRP* is equivalent isotropic radiated power. P_c is the minimum power required for chip activation, which is an inherent value when the chip is manufactured, and P_c is −20 dB m for R6 chips. P_{th} must be greater than the P_c to drive the tag. The simulated read range of the tag can be calculated by G_t and τ, and the measured results can be calculated by L_{fwd} and P_{th}.

3. Results and discussion

The GAF is prepared from GO nanosheets dispersed in GO suspension following evaporation, annealing and calendaring processes as depicted in Fig. 1a. The transmission electron microscope (TEM) image of GO nanosheets with wrinkles is shown in Fig. 1b, these wrinkles contribute to enhance the flexibility and provide a buffer for the deformation of the film. After evaporation and drying, GO nanosheets self-assembled to form GO films under the induction of hydrogen bonds. In the subsequent high-temperature

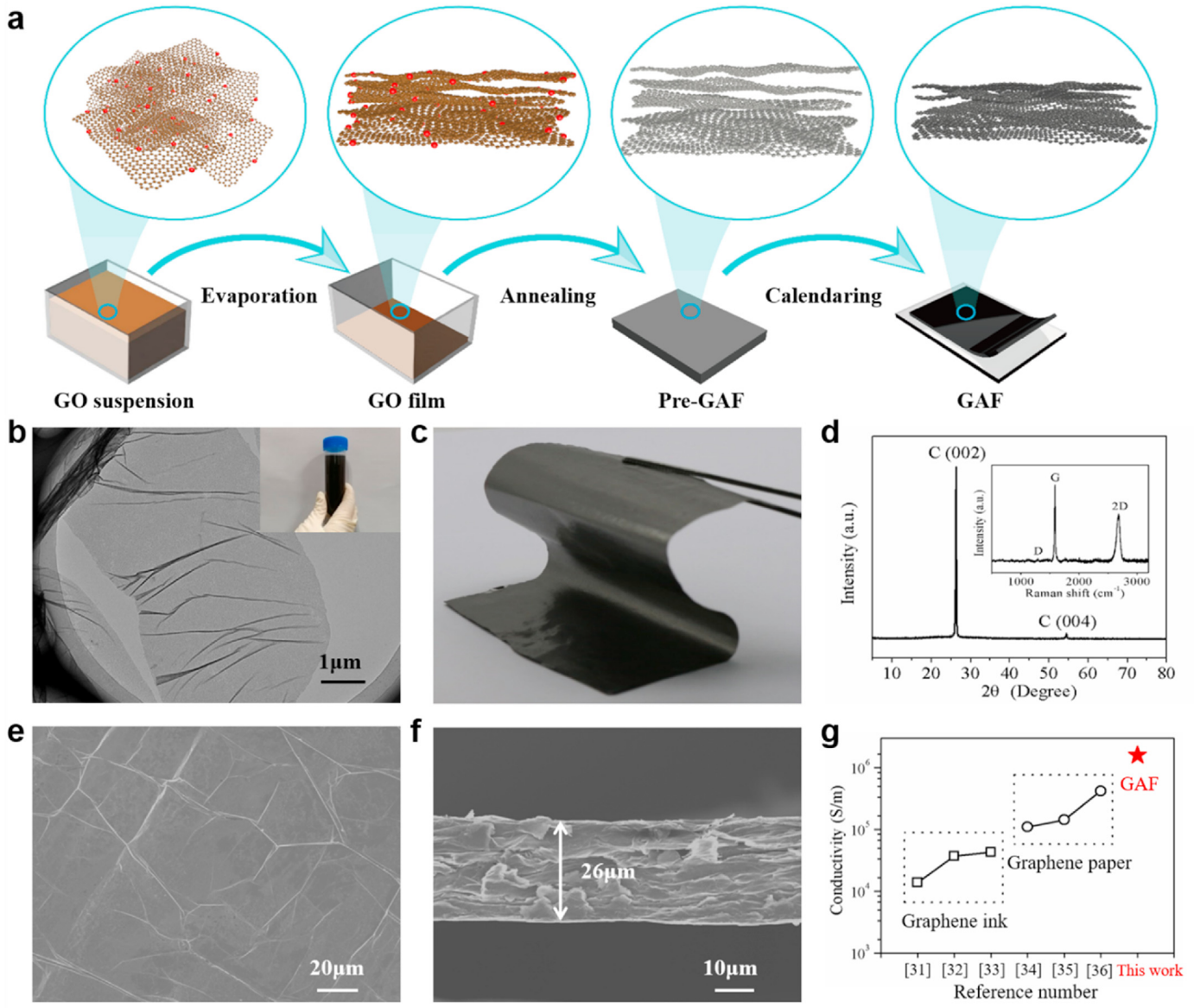

Fig. 1. Characterization of GAF. (a) Schematic illustration of GAF preparation process. (b) TEM image of GO nanosheets (inset: GO suspension). (c) Photograph of GAF. (d) XRD pattern of GAF (Inset: Raman spectrum of GAF). (e, f) SEM images of GAF surface (e) and cross-section (f). (g) Conductivity for different materials including graphene ink, graphene paper and GAF.

annealing process, the oxygen-containing groups on the GO films are transformed into gas and escape, forming a fluffy porous structure (the pre-GAF). In this structure, the lattice structure defects are reduced and sp^2 hybridization is restored. Compared with commercial highly oriented pyrolytic graphite (HOPG) and natural graphite, there is less interference during the electrons transfer process, which results in the superb conductivity of GAF. Through the static calendaring process, a thin thickness of 26 μm, low density of 1.42 g cm^3, flexible GAF (Fig. 1c) is finally formed. The ordered stacking structure can be further proved by the diffraction peak of the (004) plane in the X-ray diffraction (XRD) pattern of the GAF (Fig. 1d). The sharp diffraction peak is located at $2\theta = 26.5°$, indicating a highly graphitization structure with a layer spacing of 0.336 nm. In Raman spectroscopy (inset of Fig. 1d), the unobvious D band (1329 cm^{-1}) and strong 2D band (2684 cm^{-1}) also indicate the structure is highly graphitized. The scanning electron microscope (SEM) images of the GAF surface and cross-section are shown in Fig. 1e and f, respectively. The micro-folds on the GAF surface formed during the annealing process is beneficial to improve the flexibility of the GAF, and the thickness of the GAF is 26 μm, which is approximately twice of the skin depth δ_s at 900 MHz ($\delta_s = 14$ μm), ensuring that there is sufficient space for the electrical current to flow. A comparison of conductivity between graphene ink, graphene paper and GAF are shown in Fig. 1g, GAF with a low sheet resistance of 0.024 Ω sq^{-1} has the highest conductivity of 1.6×10^6 S m^{-1}. This means that GAF is suitable as an antenna for transmitting and receiving energy in the microwave region.

The schematic diagram of the passive RFID system and the equivalent circuit model of the RFID tag are depicted in Fig. 2a. The tag antenna receives power and data from the reader antenna and wakes up the tag chip. The tag chip modulates the backscattered signal and sends it back through the tag antenna subsequently. The power transmission coefficient τ and the antenna power reflection coefficient S_{11} describe the power transfer ratio from the antenna to

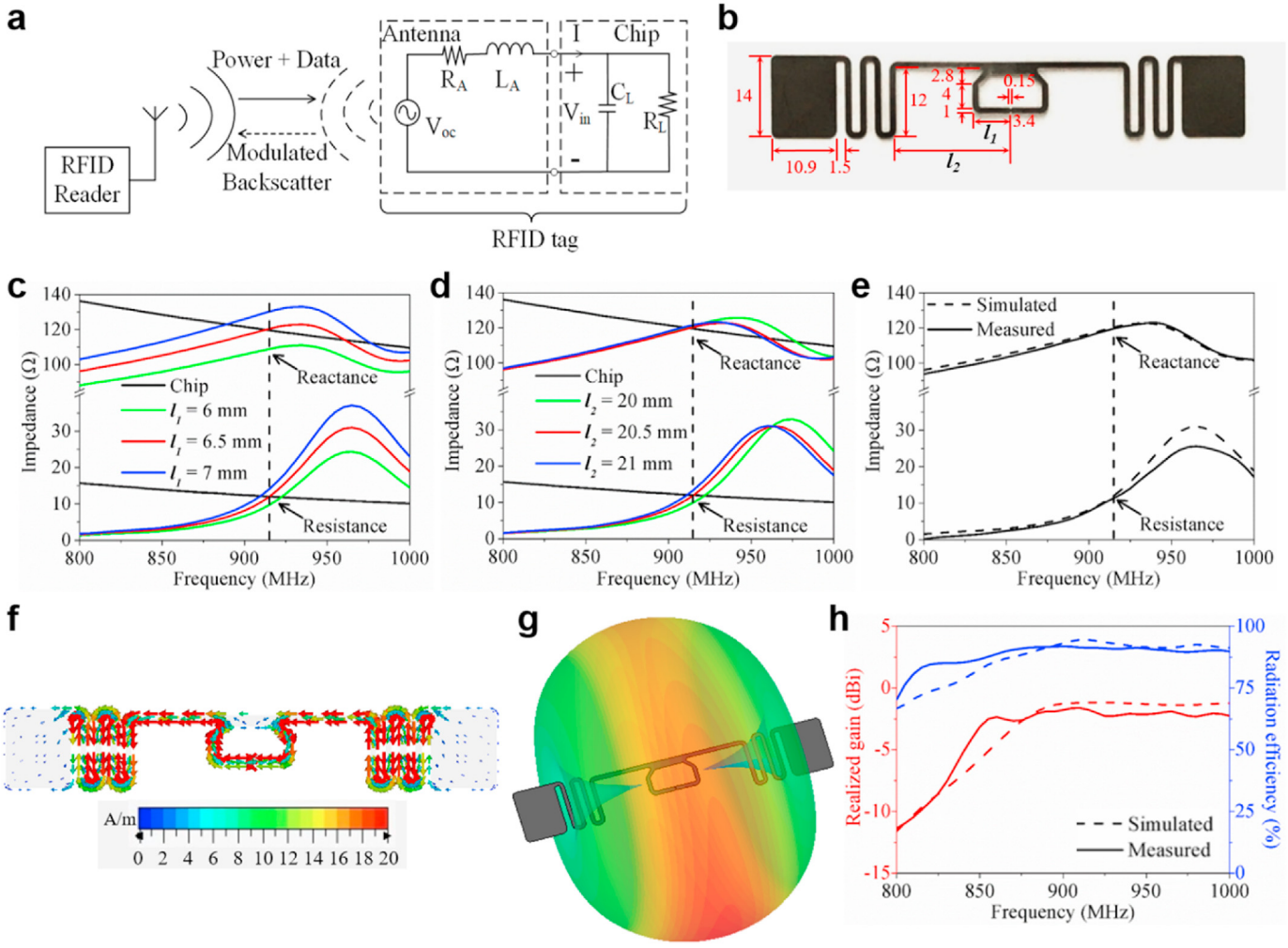

Fig. 2. Design and measurements of GAF antennas. (a) Schematic diagram of passive RFID system and equivalent circuit model of RFID tag. (b) Structure of the proposed GAF antenna with the design parameters of loop length l_1 and dipole length l_2. (c, d) Effects of different l_1 (c) and l_2 (d) on GAF antenna simulated complex impedance. (e) Simulated and measured complex impedance of GAF antenna after optimization. (f–h) Radiation performance of GAF antenna: (f) Simulated surface current distribution; (g) Simulated 3D realized gain radiation pattern; (h) Simulated and measured realized gain and radiation efficiency.

the chip [5], which is determined by:

$$\tau = 1 - |S_{11}|^2 = 1 - \left|\frac{Z_c - Z_a^*}{Z_c + Z_a}\right|^2 = \frac{4R_aR_c}{|Z_a + Z_c|^2} \quad 0 \le \tau \le 1 \tag{3}$$

where $Z_a = R_a + jX_a$ is the antenna complex impedance, and $Z_c = R_c + jX_c$ is the chip complex impedance that tends to be capacitive. In order to let the chip receive the highest power from the proposed antenna at antenna resonant frequency, according to the conjugate matching principle, Z_a needs to be equal to Zc* (conjugation of Z_c), i.e. the antenna complex impedance should be inductive.

The optimization of the GAF antenna is performed through full wave simulation with the aid of the commercial CST Microwave Studio software (Fig. 2b). As shown in Fig. 2c, the resistance and reactance of the antenna at 915 MHz (vertical dashed line) increase as loop length l_1 varies from 6 mm to 7 mm. However, the increase of dipole length l_2 only leads to the increases of the resistance, while the reactance remains unchanged (Fig. 2d). Form R6 datasheet [41], the chip is modeled by using a resistor of 1.2 kΩ and a capacitor of 1.44 pF in a parallel equivalent circuit model, which results in a complex impedance of 12 − j120 Ω at 915 MHz. When l_1 = 6.5 mm and l_2 = 20 mm, the simulated complex impedance curve (red) of the antenna and the calculated conjugate complex impedance curve (black) of the chip intersect at 915 MHz, which means that the complex impedance of the antenna is 12 + j120 Ω. This corresponds to the antenna resonating at 915 MHz with a minimum power reflection coefficient of −32 dB (Fig. S1), and a power transmission coefficient of 99.99%. Through the two-port complex impedance measurements of the antenna, the measured complex impedance agrees well with the simulated ones, verifying the optimization of the antenna (Fig. 2e, Fig. S2). To reveal the physical mechanism of the proposed antenna, the simulated surface current distribution of the antenna at 915 MHz is shown in Fig. 2f. The high current density around the loop indicates that the loop size can effectively alter the antenna radiation performance. The meander line forces the current to flow into the bending sections and thus can increase the effective length of the current path. The lengthened current path can increase the antenna resistance to achieve good conjugate matching and obtain better radiation efficiency. In the meantime, the simulated three-dimensional (3D) radiation pattern of the antenna at 915 MHz is also provided in

Fig. 2g, which is a typical radiation pattern of the dipole antenna. To investigate the practical radiation performance, the realized gain and radiation efficiency of the antenna are measured (Fig. 2h). The measured realized gain remains above −2.5 dBi across the entire UHF band (from 860 MHz to 960 MHz). The peak realized gain can reach −1.6 dBi at 910 MHz, which is slightly lower than the simulated one of −1.2 dBi, since the transmission line losses and manufacturing tolerance are not considered during the simulations. The measured radiation efficiency exceeding 90% over the entire UHF band fits well with the simulated result.

A laser machine is applied to ablate the GAF into the optimized antenna pattern with flip chip bonding and laminating procedures followed to fabricate the final GAF tag as illustrated in Fig. 3a and b. It is noted that the measured read range of the GAF tag is slightly lower than the simulated one (Fig. 3c), as the measured realized gains are lower than the simulated ones. The maximum distance in the continuous reading state with a handheld reader outdoors is 11 m (Video S1), which is 1 m lower than the measurement in the anechoic chamber, due to the influence of outdoor environmental factors and the transmission power of the handheld reader. As shown in Fig. 3d, 8-shaped 2D read range patterns, which are consistent with the simulated antenna realized gain 3D radiation pattern, can be easily observed, showing the advantage of omnidirectional radiation in the H-plane. Table 1 summarizes the material characteristics and performance of the GAF tags, compares them with previous RFID tag reports based on graphene materials, and the aluminum tag with the same GAF antenna pattern. With the highest conductivity and the lowest sheet resistance of the GAF material, even if the antenna size is smallest, the radiation efficiency of the GAF antenna and the read range of the GAF tag significantly exceed those published research works. In addition, a precise laser ablation process and stable film formation quality can complete antenna designs such as a meander line, while the published antenna designs are relatively simple dipole antenna shapes. Although the conductivity of the GAF is one order of magnitude lower than that of aluminum, the read range of the GAF tag is only 2 m lower than that of the aluminum tag.

Bending tests are carried out to demonstrate the mechanical flexibility of the GAF tags as shown in Fig. 4a, and the corresponding inset shows the GAF tag in a bent state. The antenna pattern of the aluminum tag is the same as that of the GAF tag antenna. Both tag antennas are affixed to the same PET substrate and tested at the same bending angle. The read ranges of the aluminum tag and the GAF tag at four different bending angles are shown in Fig. 4b and c, respectively. In the entire UHF band, the initial read range of the aluminum tag (without bending, $\alpha = 0°$) exceeds 12 m. With the increase of α, the read range of aluminum tag decreases more dramatically than that of GAF one in the same frequency band of 902 MHz–928 MHz, and the resonance frequency of the aluminum tag is red-shifted while the resonance frequency of the GAF tag remains basically unchanged. When α is 60°, the read range of the aluminum tag is decreased by 5 m at 915 MHz compared to the initial state. At the same state, the read range of the GAF tag is decreased by 3 m only, confirming that the GAF tag is more reliable than the aluminum tag when it is attached to a curved surface. In order to further investigate the mechanical flexibility of GAF, a rectangular GAF strip is bent to nearly 90° for repetitive cycles. It is shown that the GAF can withstand thousands of bending cycles with little change in electrical resistance (Fig. S3a). Since the conductivity of the material is determined by the electrical resistance and thickness, it can also be deduced that the conductivity of GAF remains stable before, during and after bending. Due to the π–π interactions of 2D nanosheets in the graphene layer, the 2D nanosheets can easily slide between each other along the plane and maintain huge adhesion power, leading to the remarkable electrical stability of GAF upon bending.

However, there is high stress area where the chip is bonded to the antenna, weaker adhesion can result in tag performance deterioration [42] (Fig. S3b). To verify the performance of the GAF tag after mechanical bending and stretching, the GAF tag is placed on

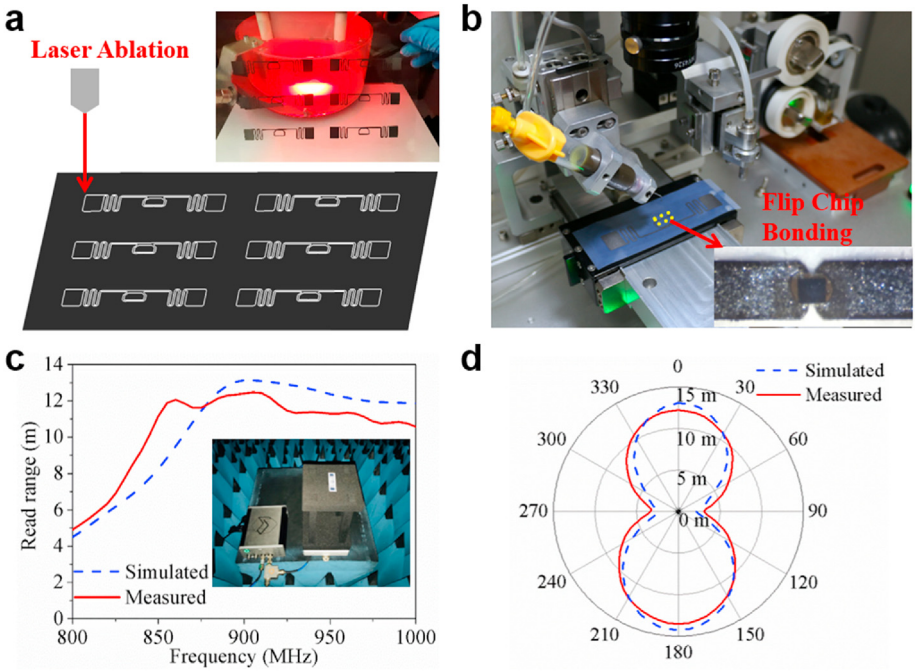

Fig. 3. Fabrication process and measurements of GAF tags. (a) Schematic diagram of laser ablated GAF antennas (inset: GAF antennas after peeling on PET substrate). (b) Flip chip bonding (inset: enlarged display of binding area). (c) Simulated and measured read range (inset: experimental setup). (d) Simulated and measured E-plane radiation pattern in terms of read range at 915 MHz.

Table 1
Summary of the parameters of graphene-based RFID tags.

Ref.	σ ($S\ m^{-1}$)	R_s ($\Omega\ sq^{-1}$)	*Antenna size (mm)*	*Efficiency*	*Read range (m)*
[28]	N/A	10	100 × 50	10%	0.2
[29]	1×10^4	5	114 × 34	N/A	2.6
[30]	4.30×10^4	3.8	92 × 25	50%	4
[31]	1.39×10^4	1.9	100 × 20	40%	5
[32]	3.7×10^4	2.88	125 × 35	51%	9
[36]	4.2×10^5	0.043	75 × 45	N/A	N/A
GAF	$(1.6 \pm 0.3) \times 10^6$	0.024 ± 0.004	81.5 × 14	90%	12
Aluminum	3.816×10^7	0.00262	81.5 × 14	97%	14

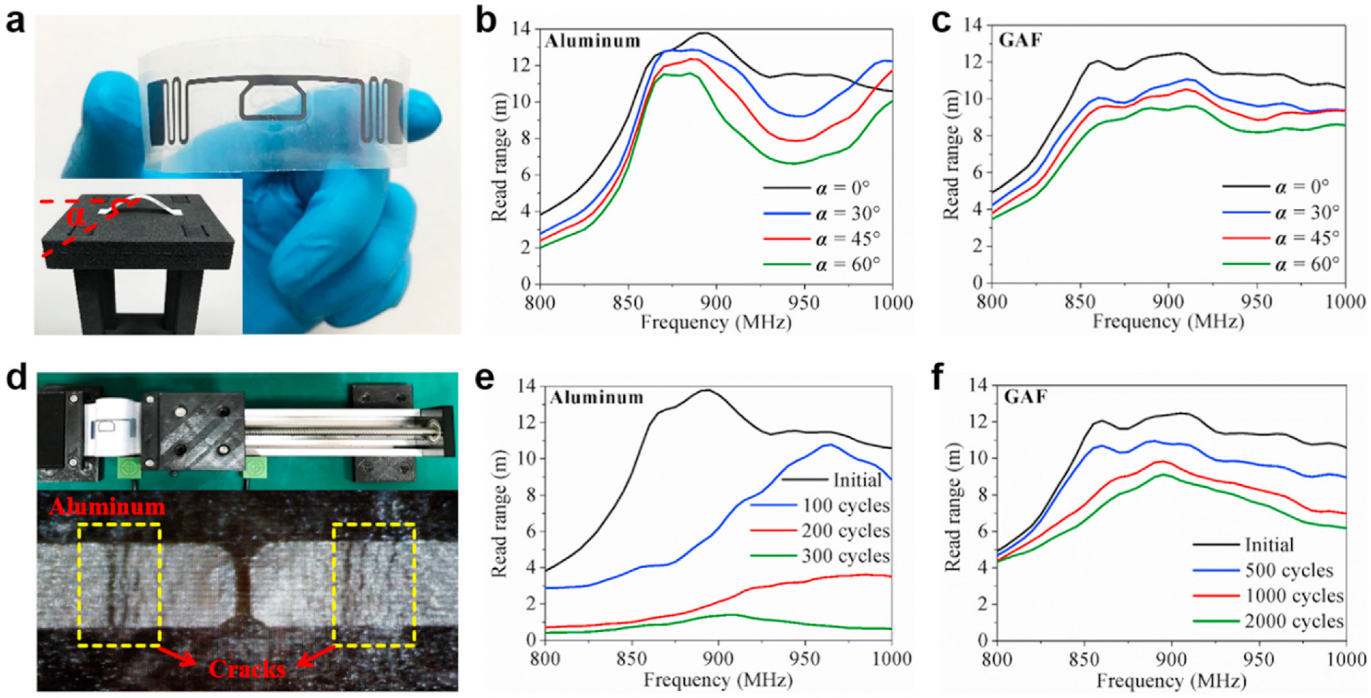

Fig. 4. Mechanical flexibility tests of GAF tag and comparison with aluminum tag. (a) Display of bending GAF (inset: experimental setup for bending test). (b, c) Read range of aluminum tag (b) and GAF tag (c) with different bending angles. (d) Experimental setup for mechanical flexibility test (upper panel). Digital photograph of cracked aluminum tag after 300 bending and stretching cycles (lower panel). (e, f) Read range of aluminum tag (e) and GAF tag (f) with different bending and stretching cycles.

the customized automatic counting slide rail (Fig. 4d, Video S2), the read range is tested after different cycles, and the same test is conducted with the aluminum tag. As shown in the lower panel of Fig. 4d, cracks occur on both sides of the aluminum tag chip bonding area within less than 300 cycles, while the GAF tag is still in good condition after 2000 cycles indicating much better mechanical stability than the aluminum tag. The resonance frequency of the aluminum tag shifts after 100 cycles, and the read range decreases to about 2 m after 200 cycles (Fig. 4e). As for the GAF tag, the read range is reduced by only 1.5 m from 12 m to 10.5 m after 500 cycles (Fig. 4f). Even after 2000 cycles, it still has a read range of 8.5 m. It indicates that the GAF tag will remain electrical percolation continuity, however the microstructure of metallic materials can be easily broken, especially in high stress area after extensive bending and stretching. The measured realized gain of the aluminum tag antenna and the GAF tag antenna after different bending and stretching cycles are shown in Fig. S4a and Fig. S4b, respectively. The realized gain measurement results of the two tag antennas are consistent with the read range of the two tags, the greater the realized gain, the longer the read range. Based on the results above, we can see that the GAF tag has excellent mechanical flexibility, showing great potential in wearable and conformal applications.

The GAF tags are pasted on five different objects, including plastic (medicine bottle), textile (clothes), cardboard (book), glass (milk bottle) and wood (blocks puzzle) as shown in Fig. S5a. The five objects are placed on a customized pallet (embedded near-field UHF reader antenna), when the object is lifted or put back from the pallet, the pickup and placement of the product marked by the tag is recorded on the display (Video S3). The measured read range of the GAF tags on five different substrates are shown in Fig. S5b. Although the read range of GAF tags that are placed on substrates with different dielectric constants and thicknesses, in the worst case, the read range can be maintained at 8 m across the UHF band, indicating that the GAF tags can satisfy the requirements for various application scenarios.

4. Conclusion

In conclusion, UHF RDIF tags are designed, fabricated, tested and demonstrated with antennas made of GAF featuring high conductivity of 1.6×10^6 S m^{-1} and low sheet resistance of 0.024 Ω sq^{-1}. Read range of ~12 m is achieved outperforming previously reported

graphene-based RFID tags even with the smallest antenna size. The flexible nature of GAF guarantees reliable performances of GAF tags when they are attached to curved surfaces. Potential application scenarios involving different substrates are also considered by attaching the GAF tags to real objects. Stable read ranges are observed demonstrating the wide applicability of the GAF tags. These results provide possible solutions for metal replacement in UHF RFID tags and many other related applications.

CRediT authorship contribution statement

Bohan Zhang: Conceptualization, Methodology, Writing – original draft. **Zhe Wang:** Resources. **Rongguo Song:** Data curation. **Huaqiang Fu:** Formal analysis. **Xin Zhao:** Writing – review & editing. **Cheng Zhang:** Validation. **Daping He:** Funding acquisition, Supervision. **Zhi P. Wu:** Project administration.

Declaration of competing interest

The authors declare that they have no known competing financial interests or personal relationships that could have appeared to influence the work reported in this paper.

Acknowledgements

This work is financially supported by 2018 National Key R&D Program of China (No. 257), the National Natural Science Foundation of China (No. 51572205), the Equipment Pre-Research Joint Fund of EDD and MOE (No. 614A02022262).

Appendix A. Supplementary data

Supplementary data to this article can be found online at https://doi.org/10.1016/j.carbon.2021.02.096.

References

[1] K. Finkenzeller, RFID Handbook: Fundamentals and Applications in Contactless Smart Cards, Radio Frequency Identification and Near-Field Communication, John Wiley & Sons, New Jersey, 2010.
[2] A. Juels, RFID security and privacy: a research survey, IEEE J. Sel. Area. Commun. 24 (2006) 381–394.
[3] C. Occhiuzzi, S. Caizzone, G. Marrocco, Passive UHF RFID antennas for sensing applications: principles, methods, and classifcations, IEEE Antenn. Propag. Mag. 55 (2013) 14–34.
[4] J. Zhang, G.Y. Tian, A.M.J. Marindra, A.I. Sunny, A.B. Zhao, A review of passive RFID tag antenna-based sensors and systems for structural health monitoring applications, Sensors 17 (2017) 265.
[5] K.V.S. Rao, P.V. Nikitin, S.F. Lam, Antenna design for UHF RFID tags: a review and a practical application, IEEE Trans. Antenn. Propag. 53 (2005) 3870–3876.
[6] G. De Vita, G. Iannaccone, Design criteria for the RF section of UHF and microwave passive RFID transponders, IEEE Trans. Microw. Theor. Tech. 53 (2005) 2978–2990.
[7] G. Marrocco, The art of UHF RFID antenna design: impedance-matching and size-reduction techniques, IEEE Antenn. Propag. Mag. 50 (2008) 66–79.
[8] V. Forti, C.P. Balde, R. Kuehr, G. Bel, The Global E-Waste Monitor 2020: Quantities, Flows and the Circular Economy Potential, United Nations University, United Nations Institute for Training and Research, International Telecommunication Union, and International Solid Waste Association, Bonn, Geneva, Rotterdam, 2020.
[9] S. Higginbotham, The internet of trash (Internet of everything), IEEE Spectr 55 (2018), 17–17.
[10] C. Rutherglen, D. Jain, P. Burke, Nanotube electronics for radiofrequency applications, Nat. Nanotechnol. 4 (2009) 811–819.
[11] E. Amram Bengio, D. Senic, L.W. Taylor, R.J. Headrick, M. King, P. Chen, et al., Carbon nanotube thin film patch antennas for wireless communications, Appl. Phys. Lett. 114 (2019), 203102.
[12] A. Galehdar, P.J. Callus, W.S.T. Rowe, C. Wang, S. John, K. Ghorbani, Capacitively fed cavity-backed slot antenna in carbon-fiber composite panels, IEEE Antenn. Wireless Propag. Lett. 11 (2012) 1028–1031.
[13] R. Song, Q. Wang, B. Mao, Z. Wang, D. Tang, B. Zhang, et al., Flexible graphite films with high conductivity for radio-frequency antennas, Carbon 130 (2018) 164–169.
[14] R. Kato, M. Hasegawa, Fast synthesis of thin graphite film with high-performance thermal and electrical properties grown by plasma CVD using polycrystalline nickel foil at low temperature, Carbon 141 (2019) 768–773.
[15] K.S. Novoselov, A.K. Geim, S.V. Morozov, D. Jiang, Y. Zhang, S.V. Dubonos, et al., Electric field effect in atomically thin carbon films, Science 306 (2004) 666–669.
[16] A.K. Geim, K.S. Novoselov, The rise of graphene, Nat. Mater. 6 (2007) 183–191.
[17] W. Ren, H.M. Cheng, The global growth of graphene, Nat. Nanotechnol. 9 (2014) 726–730.
[18] E.P. Randviir, D.A.C. Brownson, C.E. Banks, A decade of graphene research: production, applications and outlook, Mater. Today 17 (2014) 426–432.
[19] M. Dragoman, A.A. Muller, D. Dragoman, F. Coccetti, R. Plana, Terahertz antenna based on graphene, J. Appl. Phys. 107 (2010), 104313.
[20] Z. Xu, X. Dong, J. Bornemann, Design of a reconfigurable MIMO system for THz communications based on graphene antennas, IEEE Trans. Terahertz Sci. Technol. 4 (2014) 609–617.
[21] X. Du, I. Skachko, A. Barker, E.Y. Andrei, Approaching ballistic transport in suspended graphene, Nat. Nanotechnol. 3 (2008) 491–495.
[22] S. Bae, H. Kim, Y. Lee, X. Xu, J.S. Park, Y. Zheng, et al., Roll-to-roll production of 30-inch graphene films for transparent electrodes, Nat. Nanotechnol. 5 (2010) 574–578.
[23] Y. Zhu, S. Murali, W. Cai, X. Li, J.W. Suk, J.R. Potts, et al., Graphene and graphene oxide: synthesis, properties, and applications, Adv. Mater. 22 (2010) 3906–3924.
[24] X. Huang, Z. Yin, S. Wu, X. Qi, Q. He, Q. Zhang, et al., Graphene-based materials: synthesis, characterization, properties, and applications, Small 7 (2011) 1876–1902.
[25] A.J. Marsden, D.G. Papageorgiou, C. Vallés, A. Liscio, V. Palermo, M.A. Bissett, et al., Electrical percolation in graphene–polymer composites, 2D Mater. 5 (2018), 032003.
[26] K.Y. Shin, J.Y. Hong, J. Jang, Micropatterning of graphene sheets by inkjet printing and its wideband dipole-antenna application, Adv. Mater. 23 (2011) 2113–2118.
[27] T.T. Tung, S.J. Chen, C. Fumeaux, D. Losic, Scalable realization of conductive graphene films for high-efficiency microwave antennas, J. Mater. Chem. C 4 (2016) 10620–10624.
[28] P. Kopyt, B. Salski, M. Olszewska-Placha, D. Janczak, M. Sloma, T. Kurkus, et al., Graphene-based dipole antenna for a UHF RFID tag, IEEE Trans. Antenn. Propag. 64 (2016) 2862–2868.
[29] K. Arapov, K. Jaakkola, V. Ermolov, G. Bex, E. Rubingh, S. Haque, et al., Graphene screen-printed radio-frequency identification devices on flexible substrates, Phys. Status Solidi RRL – Rapid Res. Lett. 10 (2016) 812–818.
[30] T. Leng, X. Huang, K.H. Chang, J.C. Chen, M.A. Abdalla, Z. Hu, Graphene nanoflakes printed flexible meandered-line dipole antenna on paper substrate for low-cost RFID and sensing applications, IEEE Antenn. Wireless Propag. Lett. 15 (2016) 1565–1568.
[31] M. Akbari, M.W.A. Khan, M. Hasani, T. Björninen, L. Sydänheimo, L. Ukkonen, Fabrication and characterization of graphene antenna for low-cost and environmentally friendly RFID tags, IEEE Antenn. Wireless Propag. Lett. 15 (2016) 1569–1572.
[32] K. Pan, Y. Fan, T. Leng, J. Li, Z. Xin, J. Zhang, et al., Sustainable production of highly conductive multilayer graphene ink for wireless connectivity and IoT applications, Nat. Commun. 9 (2018) 5197.
[33] X. Huang, T. Leng, X. Zhang, J.C. Chen, K.H. Chang, A.K. Geim, et al., Binder-free highly conductive graphene laminate for low cost printed radio frequency applications, Appl. Phys. Lett. 106 (2015), 203105.
[34] P. Li, M. Yang, Y. Liu, H. Qin, J. Liu, Z. Xu, et al., Continuous crystalline graphene papers with gigapascal strength by intercalation modulated plasticization, Nat. Commun. 11 (2020) 2645.
[35] L. Paliotta, G. De Bellis, A. Tamburrano, F. Marra, A. Rinaldi, S.K. Balijepalli, et al., Highly conductive multilayer-graphene paper as a flexible lightweight electromagnetic shield, Carbon 89 (2015) 260–271.
[36] A. Scidà, S. Haque, E. Treossi, A. Robinson, S. Smerzi, S. Ravesi, et al., Application of graphene-based flexible antennas in consumer electronic devices, Mater, Today Off. 21 (2018) 223–230.
[37] W. Zhou, C. Liu, R. Song, X. Zeng, B.W. Li, W. Xia, et al., Flexible radiofrequency filters based on highly conductive graphene assembly films, Appl. Phys. Lett. 114 (2019), 113503.
[38] J. Zhang, R. Song, X. Zhao, R. Fang, B. Zhang, W. Qian, et al., Flexible graphene-assembled film-based antenna for wireless wearable sensor with miniaturized size and high sensitivity, ACS Omega 5 (2020) 12937–12943.
[39] X. Qing, C.K. Goh, Z.N. Chen, Impedance characterization of RFID tag antennas and application in tag co-design, IEEE Trans. Microw. Theor. Tech. 57 (2009) 1268–1274.
[40] P.V. Nikitin, K.V.S. Rao, R. Martinez, S.F. Lam, Sensitivity and impedance measurements of UHF RFID chips, IEEE Trans. Microw. Theor. Tech. 57 (2009) 1297–1302.
[41] Impinj datasheet Monza R6. https://support.impinj.com/hc/en-us/articles/202765328-Monza-R6-Product-Datasheet.
[42] K. Janeczek, M. Jakubowska, G. Kozioł, A. Młożniak, Electrical and mechanical properties of RFID chip joints assembled on flexible substrates, Solder. Surf. Mt. Technol. 27 (2015) 13–21.